NANO LETTERS

Letter

pubs.acs.org/NanoLett

# Nanostructured Clathrate Phonon Glasses: Beyond the Rattling Concept

Yuping He[†] and Giulia Galli*[,‡]

[†]Department of Chemistry, University of California, Davis, California 95616, United States

[‡]The Institute for Molecular Engineering, The University of Chicago, Chicago, Illinois 60637, United States

**ABSTRACT:** Using first-principles calculations, we investigated the thermoelectric properties of a newly synthesized Si-based ternary clathrate $K_8Al_8Si_{38}$, composed of ∼1 nm hollow cages with a metal atom inside. This compound contains solely Earth abundant elements. We found that, similar to other nanostructured type I clathrates, this system is a semiconductor and has a low thermal conductivity (∼1 W/mK). It was long believed that the mere presence of rattling centers was responsible for the low lattice thermal conductivity of type I clathrates. We found instead that the cage structural disorder induced by atomic substitution plays a crucial role in determining the conductivity of these materials, in addition to the dynamics of the guest atoms. Our calculations showed that the latter is substantially affected by the charge transfer between the metal and the cages. Our results provide design rules for the search of new types of promising nanocage structured thermoelectric materials.

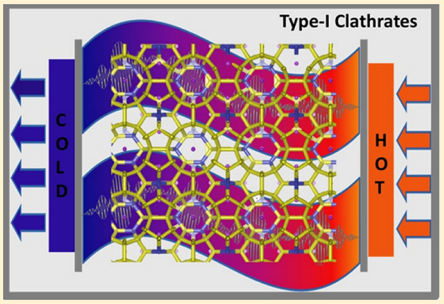


**KEYWORDS:** *Nanostructured clathrates, phonons, thermal conductivity, first-principles calculations*

Solid-state thermoelectric generators[1−3] are expected to play a key role in improving vehicle fuel efficiency by transforming waste heat into electricity and, in their cooling mode, by replacing green house gases used in air-conditioning devices. The efficiency of thermoelectric (TE) conversion of heat and electricity by solid-state systems is determined by the figure of merit $ZT = \sigma S^2 T/(\kappa_e + \kappa_L)$, where $\sigma$ is the electrical conductivity, $S$ the Seebeck coefficient, $T$ the temperature, and $\kappa_e$ and $\kappa_L$ are the electronic and ionic contributions to the thermal conductivity, respectively. A material behaving as a phonon-glass and an electron-crystal (PGEC),[4] i.e., exhibiting low thermal conductivity and good electron conduction properties, would be ideal to achieve a high ZT.

Nanostructured type I clathrates composed of cages of group III and IV elements, and either alkaline-earth or alkali guest atoms (see Figure 1), have long been considered as promising PGEC systems. More than a decade ago Nolas et al.[5,6] showed that for 5 K ≤ $T$ ≤ 300 K, the behavior of the thermal conductivity of $Sr_8Ga_{16}Ge_{30}$ as a function of $T$ resembles that of a glass, and they suggested that the low values of $\kappa_L$ were determined by the rattling modes of the Sr atoms. Several subsequent theoretical studies[7−10] supported this hypothesis. In 2006, Okamoto et al.[11,12] investigated the relationship between rattling modes and $\kappa_L$ in $Ba_8Ga_xSi_{46-x}$ using synchrotron X-ray powder diffraction. They concluded that the splitting of guest atom sites is responsible for lowering the phonon lifetimes and thus $\kappa_L$. Christensen et al.[13] suggested instead that the motion of rattling atoms contributed to a substantial flattening of the host material phonon curves, rather than to a lowering of its phonon lifetimes. Recently Fujiwara and co-workers[14] investigated $X_8Ga_{16}Ge_{30}$ (X = Sr, Ba) and proposed that the coupling of the motion of the guest atoms and the host cage may help reduce $\kappa_L$.

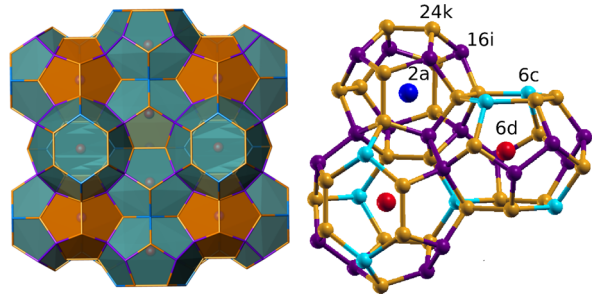


**Figure 1.** Ball and stick representation of the type I clathrate $K_8Al_8Si_{38}$. Left panel: dodecahedral and tetrakaidecahedral cages composing the material. Right panel: Wyckoff sites of the structure; the center of the cages are denoted by 2*a* (blue) and 6*d* (red) for dodecahedral and tetrakaidecahedral cages, respectively, and the host structure is represented by three inequivalent crystallographic sites, 6*c* (cyan), 16*i* (purple), and 24*k* (orange). The diameter of the cage is ∼0.6 nm.

Most experimental and theoretical studies to date focused on the role of rattling guest atoms in determining the lattice thermal conductivity of ternary clathrates; the dynamical properties of the host structure received much less attention, in spite of the interesting suggestions on the cage dynamics in the case of *binary* clathrates[15] and of conjectures on host structure occupancies[16] and electron−phonon interaction.[17] Experimentally, it is difficult to probe the dynamical properties

**Received:** March 18, 2014
**Revised:** April 15, 2014
**Published:** April 24, 2014

   dx.doi.org/10.1021/nl501021m | *Nano Lett.* 2014, 14, 2920−2925

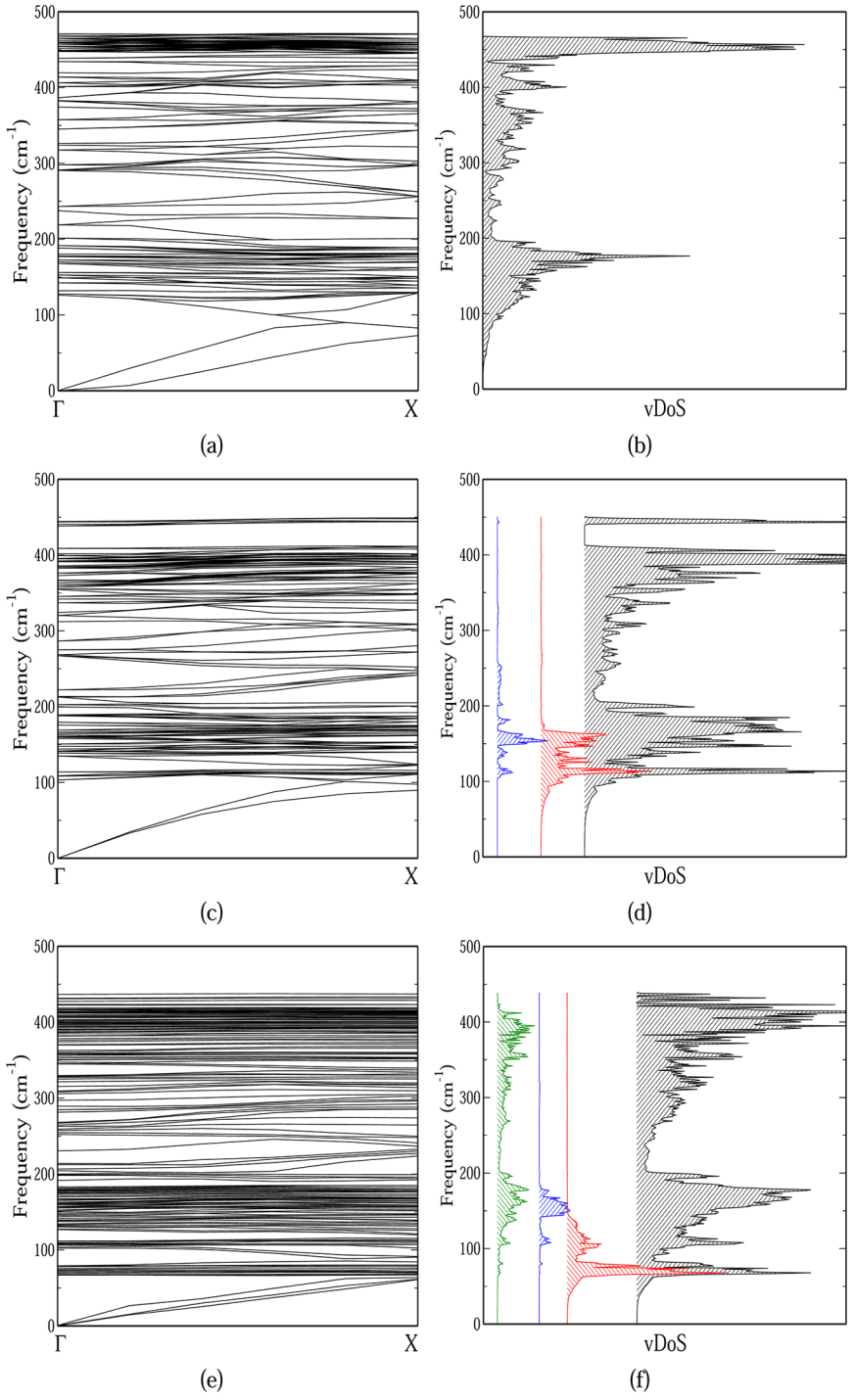


**Figure 2.** Phonon dispersion curves along the Γ−X direction (panels a, c, and e) and density of states (vDoS) contributed from different sites (panels b, d, and f) for $Si_{46}$ (upper panels), $K_8Si_{46}$ (middle panels), and $K_8Al_8Si_{38}$ (lower panels). The red (blue) lines represent the partial vDoS contributed by K in the large (small) cages (*6d* (*2a*) sites; see Figure 1); the green line represents the partial vDoS contributed by the Al atoms. Note that the VDoS contributions of K are not zero at high frequency, but much smaller than that of the Al atoms and hence appear to be vanishingly small on the scale of the figure.

of cages composed of elements with similar atomic numbers (e.g., Ga and Ge or Al and Si). It is therefore of great interest to use first-principles methods to elucidate the nature of the low thermal conductivity in ternary clathrates.

In this letter, we focused on the type I clathrate $K_8Al_8Si_{38}$, composed entirely of Earth abundant elements. While most of the ternary clathrates proposed in the literature for thermoelectric applications are Ge-based,[7,16−21] here we considered a Si-based system, which holds the promise of cheaper solid-state thermoelectric devices. We generated a model of $K_8Al_8Si_{38}$, starting from data obtained from XRD measurements.[22] We then computed the electronic and vibrational properties of these models, as well as the thermal conductivity. Our computed phonon density of states, together with a detailed analysis of partial vibrational density of states, allowed us to elucidate the prominent role of cage structural disorder in


dx.doi.org/10.1021/nl501021m | *Nano Lett.* 2014, 14, 2920−2925

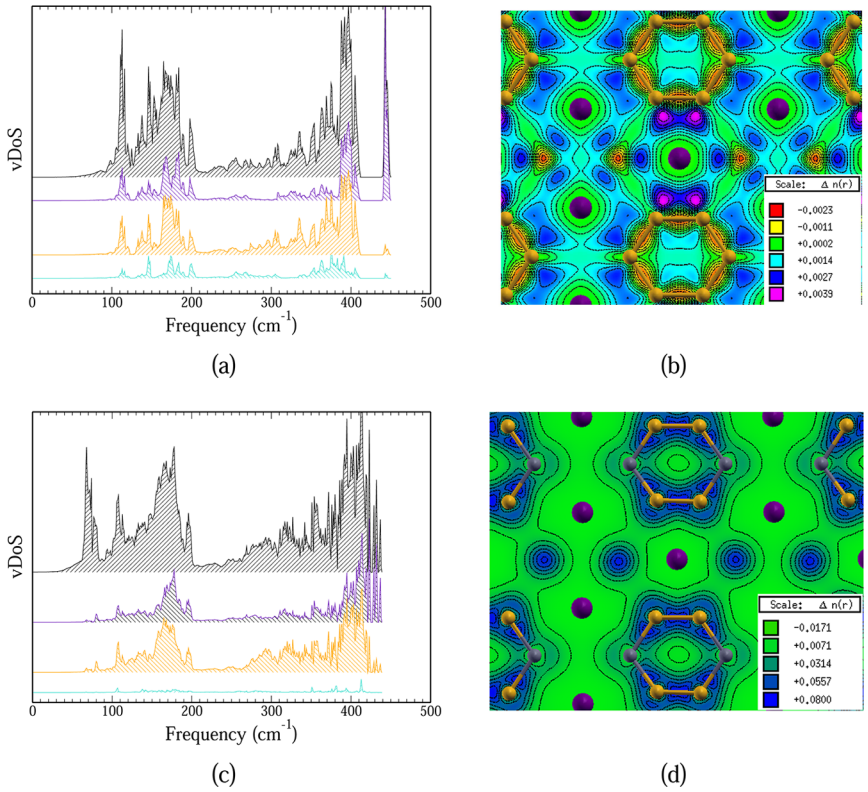


**Figure 3.** Partial vibrational density of states (vDoS) (left panels) and electronic charge density plots (right panels, in units of elementary electronic charge) of $K_8Si_{46}$ (upper panels) and $K_8Al_8Si_{38}$ (lower panels). In the vDoS of $K_8Si_{46}$ (a) and $K_8Al_8Si_{38}$ (c), the purple (orange) lines represent the contribution from Si atoms at 16*i* (24*k*) sites; the cyan lines represent the contribution from Si atoms at 6*c* sites. In the right panels we show the charge density difference $\Delta n = n(K_8Si_{46}) - n(Si_{46})$ (b) and $\Delta n = n(K_8Al_8Si_{38}) - n(Al_8Si_{38})$ (d), where $n$ denotes the electronic charge density and $n(Si_{46})$ and $n(Al_8Si_{38})$ are computed at the geometry of $K_8Si_{46}$ and $K_8Al_8Si_{38}$, respectively. Potassium, silicon, and aluminum atoms are represented by magenta, yellow, and gray, respectively.

determining the lattice thermal conductivity; futhermore, we examined the effect of charge transfer between metal guest atoms and host cages by analyzing electronic charge densities.

The configurations of all Si-based type I clathrates were generated starting from the geometry of $Si_{46}$[23] in the cubic space group $Pm\bar{3}n$. We then inserted K atoms into the eight cages to obtain a model of $K_8Si_{46}$,[24] and randomly substituted eight Si with Al atoms over the three Wyckoff sites: 6*c*, 16*i*, and 24*k* to obtain $K_8Al_8Si_{38}$ with an ideal stoichiometric ratio. All sample geometries were optimized with respect to the volume and atomic positions using first-principles density functional theory (DFT)[25] within the generalized gradient approximation of Perdew–Burke–Ernerhof (PBE-GGA),[26,27] plane wave basis sets, and norm-conserving pseudopotentials.[28]

We generated six snapshots using the guidelines for site occupancy proposed by Christensen et al.[29] These are 6*c*2*i*, 5*c*2*k*1*i*, 8*k*, 3*c*5*i*, 3*c*5*k*, and 8*i*, where the letters denote atomic sites and the digits denote the number of sites occupied by Al atoms. We then computed the total energies of the six samples and identified the two most stable configurations: 6*c*2*i* and 5*c*2*k*1*i*. These results are consistent with those recently observed experimentally in the type I clathrate $Ba_8Al_xSi_{46-x}$[30] and with those found in the single crystal $K_8Al_8Si_{38}$ grown by a simple mixing and baking method.[22] We found that not only the value of site distances but also the relative order of distances obtained by first-principles optimizations is in satisfactory agreement with experimental results, indicating that the lowest energy models generated using ab inito calculations are adequate to represent the structure of type I clathrate obtained in experiments. The lattice constant of the optimized model is 1.06 nm, i.e., 0.9% larger than the measured value (1.05 nm).[22]

To investigate the origin of the thermal conductivity of the $K_8Al_8Si_{38}$ clathrate, we compared the dispersion curves, and the total and partial vibrational density of states (vDoS) of the $Si_{46}$, $K_8Si_{46}$, and $K_8Al_8Si_{38}$ crystals, which were obtained using first-principles density functional perturbation theory (DFPT).[31−33] The partial vDoS on a given atoms "*i*" was computed from the total vDoS using the definition:

$$N_i(E) = \sum_{j=1}^{n} \int \frac{d\mathbf{k}}{4\pi^3} \left| \mathbf{e}_j(i) \right|^2 \delta(E - E_j(\mathbf{k}))$$

where $j$ denotes a phonon band, and $\mathbf{e}_j$ is the eigenvector associated with the phonon mode of energy $E_j(\mathbf{k})$ at the wave vector $\mathbf{k}$. In the case of $K_8Al_8Si_{38}$, we chose the 5*c*2*k*1*i* model, which best fits the experimental structural data.[22] As shown in Figure 2a, $Si_{46}$ has a smaller ratio of acoustic to total number of modes with respect to , e.g., diamond Si,[34] and its thermal conductivity is expected to be substantially reduced compared to that of bulk Si. In addition (see Figure 2b), the computed vDoS of $Si_{46}$ shows that its optical branches shift to lower frequencies with respect to the corresponding ones in diamond Si,[34] likely because of the slight disorder present in the clathrate structure:[35] acoustic branches shift instead to higher frequencies. The difference between the dispersion curves of $Si_{46}$ and diamond Si obtained here is similar to that between $Ge_{46}$ and diamond Ge reported by Dong et al.[9]


dx.doi.org/10.1021/nl501021m | Nano Lett. 2014, 14, 2920−2925

Figure 2c,d shows the effect, on the vibrational states of $Si_{46}$, of the presence of potassium: inserting K in the cages, leads to the appearance of few isolated high frequency modes (>400 $cm^{-1}$) and to the flattening of several bands around 100 $cm^{-1}$, consistent with the findings of ref 9 on Ge-based binary clathrates. After substituting Si with Al the high frequency modes of K cease to be isolated, and a multitude of additional flat bands appear at ~70 $cm^{-1}$ (see Figure 2e,f). To identify and separate the effects of rattling K atoms and substitutional Al atoms on the features observed in the dispersion curves, we computed the partial vibrational density of states arising from K belonging to the large (K-6*d*) and small (K-2*a*) cages for both $K_8Si_{46}$ and $K_8Al_8Si_{38}$, and in the latter case from Al atoms at all sites (6*c*, 24*k*, and 16*i*). We emphasize that it is key to analyze not only the total vDoS but also the partial density of states to identify the complex coupling between rattler and cage modes. In the case of $K_8Si_{46}$, we found that K-6*d* sites (shown in red in Figure 2d) contribute to both acoustic and optical modes, for frequencies smaller than 170 $cm^{-1}$, i.e., in a frequency range overlapping with those of the host lattice modes. Hence there is a coupling between the K-6*d* site rattling modes and the vibrations of the cages; instead the K-2*a* sites only contribute (see blue curve in Figure 2d) to optical modes in the interval 100−250 $cm^{-1}$. Note that some of the rattling mode frequencies are higher than those of the acoustic phonon frequencies of the host lattice. Hence the occurrence of flat bands in $K_8Si_{46}$ can be clearly related to the vDoS contributions from K-6*d* and K-2*a* sites.

In the case of $K_8Al_8Si_{38}$, we found that the substitution of Si with Al shifts the rattling modes of K-6*d* sites (red line in Figure 2f) to lower frequencies (70 $cm^{-1}$), leading to the overlap with the acoustic phonons of the host lattice. The mode shift observed here is consistent with that reported experimentally for another clathrate, $Ba_8Ge_{40+x}Ni_{6-x}$, using neutron diffraction.[36] We expect that such overlap induces anticrossings in phonon bands between the rattling and host acoustic branches, leading to a significant decrease of the group velocity of the host acoustic phonons, which is likely responsible for a reduction of the thermal conductivity. These results show that one of the key reasons responsible for the microscopic origin of the low thermal conductivity in ternary clathrates is the presence of Al in the cages and hence of compositional disorder.

To further understand the effect of the bonding properties of $K_8Al_8Si_{38}$ on the phonon density of states, we analyzed the electronic charge density distribution in proximity of the K atoms in both $K_8Si_{46}$ and $K_8Al_8Si_{38}$ (see Figure 3). We found that in the absence of Al, the compound is metallic, while it is semiconducting when Al is present, with a band gap close to that of bulk Si.[22] In $K_8Si_{46}$, we found that K atoms are forming covalent-like bonds with all Si in the small cages, and with Si atoms belonging to the six-membered rings of the large cages. Bonds with the remaining atoms in the large cages appear to be much weaker. This is illustrated in Figure 3b, which shows the charge density difference between the $K_8Si_{46}$ and the $Si_{46}$ crystals, where in the latter all Si atoms are in the same positions as in the former. These results can be rationalized using simple geometric criteria, indicating, as expected, that the overlap between the charge on the K and Si atoms is maximized in the small cages. Indeed the sum of the atomic radii of K (~0.22 nm) and Si (~0.11 nm) is larger than the radius of the small cages (0.3 nm). It is also larger (smaller) than that of the large cage along the direction perpendicular (parallel) to the six-membered ring planes (0.25 nm (0.35 nm)). The formation of covalent-like K−Si bonds is most likely responsible for the coupling of the rattling modes with the vibrations of the host lattice in $K_8Si_{46}$; these findings are consistent with those of refs 10 and 35 where the authors showed that the vDOS of guest atoms of different ionic radii exhibited different overlaps with that of the host lattice.

Figure 3d reports the electronic charge density difference between $K_8Al_8Si_{38}$ and $Al_8Si_{38}$, and it illustrates that the presence of Al makes the bonds between the guest metal and the cage more ionic than in $K_8Si_{46}$. Indeed, Al forms three bonds with Si, thus leaving a dangling bond, which can easily accept charge from the guest K. The metal atom is thus present in an ionic form in the cage (although it is not necessarily fully ionized), and the coupling of its dynamics with that of the host lattice is decreased, consistent with the suggestions of ref 14 where the authors proposed that the host−guest atoms coupling is inversely proportional to their electrostatic interaction. Our results are also consistent with the charge transfer discussion reported by Gatti et al.[18] on a chemically similar compounds $Sr_8Ga_{30}Ge_{30}$. Importantly, our results showed for the first time that it is the disorder induced by Al that further shifts the isolated rattling modes to lower frequency with respect to the vibrations of the host lattice.[37] These shifted modes scatter and retard the acoustic vibrations of the cages, leading to a reduction of the lattice thermal conductivity. It is thus not sufficient just to have rattling guest atoms to account for a low thermal conductivity. A certain amount of structural disorder in the cages is necessary to shift the rattling modes to low frequencies. We note that the computed vDoS of K-6*d* and K-2*a* sites still exhibit some overlap between K and Al states (see Figure 2f), indicating the presence of a coupling, albeit small, between the guest metals and the host lattice.

To analyze whether the isolated high frequency modes in the vDoS of $K_8Si_{46}$ are related to the weaker bonds between K and the large cage Si atoms, we computed the partial vDoS of Si occupying 16*i*, 24*k*, and 16*c* sites, for both $K_8Si_{46}$ and $K_8Al_8Si_{38}$. As shown in Figure 3a, we found that most of the isolated high frequency modes are from Si at 16*i* sites, with some contributions from Si atoms at 24*k* and 6*c* sites. After substitution of Si with Al, the ionicity of K−Si bonds increases in $K_8Al_8Si_{38}$ (see Figure 3d), leading to a red shift of the modes originally isolated in $K_8Si_{46}$ (see Figure 3c).

Since the rattling modes are coupled with those of the host lattice in $K_8Si_{46}$, but largely decoupled in $K_8Al_8Si_{38}$, we expect that the lattice thermal conductivity of $K_8Si_{46}$ be larger than that of $K_8Al_8Si_{38}$. We computed $\kappa_L$ as a function of the average value of the vibrational mean free path ($\bar{L}$) for both compounds, using a kinetic model:

$$\kappa_L = \frac{1}{3} C_V v_s \bar{L}$$

where $C_V$ is the volumetric heat capacity, $v_s$ is the speed of sound, and $\bar{L}$ is an estimated average value of mean free path.[38] Although approximate, a kinetic model is useful to obtain qualitative differences between the conductivity of the compounds with and without Al. We derived $C_V$ from the integral of the phonon density of states over the whole frequency spectrum:

$$C_V = \frac{k_B}{V} \int_0^\infty g(\nu) x^2 \frac{e^x}{(e^x - 1)^2} d\nu$$


dx.doi.org/10.1021/nl501021m | Nano Lett. 2014, 14, 2920−2925

with $x = (h\nu)/(k_B T)$, and we estimated $v_s$ as an average group velocities of one longitudinal and two transverse acoustic modes at the Γ point. We then varied the average mean free path of the phonons entering the expression of the thermal conductivity in an interval of distances close to the cage diameters, to determine the qualitative difference between the conductivity of the clathrate with and without the positional disorder induced by Al. As shown in Figure 4, using this range

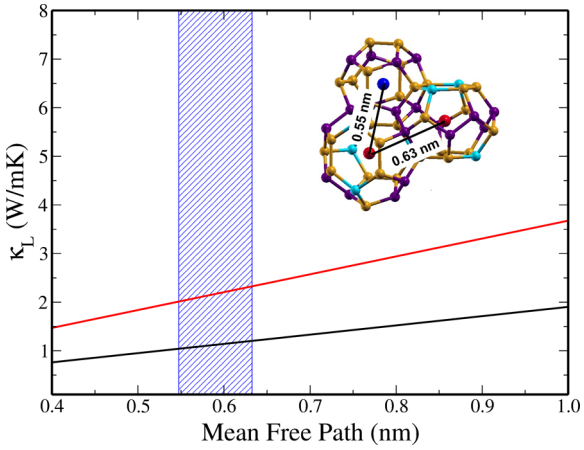


**Figure 4.** Computed lattice thermal conductivity ($\kappa_L$) of $K_8Al_8Si_{38}$ (black) and $K_8Si_{46}$ (red) as a function of the average mean free path. The shaded area represents the range of K−K distance present in the sample (see text). The ball and stick representation of the cages is the same as that in Figure 1

of mean free paths, we found that the $\kappa_L$ of $K_8Si_{46}$ is always substantially larger than that of $K_8Al_8Si_{38}$. These results indicate that the disorder induced from Al substitution plays a key role in reducing the clathrate thermal conductivity. Our computed value of $\kappa_L$ for $K_8Al_8Si_{38}$ is consistent with recent measurements carried out at 300 K that gave a total value of $\kappa_T \approx 1.7$ W/mK ($\kappa_T = \kappa_e + \kappa_L$).[39] It is also in accord with the value of $\kappa_L$ reported for $K_8Al_8Sn_{38}$ (1.2 W/mK).[40]

In summary, we showed that the rattling concept, widely used in the literature of the last two decades, is insufficient to understand the origin of the low thermal conductivity in nanostructured type I clathrates. We employed a combination of experimental (XRD) data[22] and ab initio calculations to derive a structural model for the newly synthesized $K_8Al_8Si_{38}$ clathrate; the model was then used to compute vibrational and thermoelectric properties. We showed that rattlers may vibrate in qualitatively different manners, depending on whether they are surrounded by ordered or disordered cages. We found that it is the presence of substitutional disorder in the host cages that leads to a decoupling of the rattler modes with those of the cages and hence to a reduction of the thermal conductivity. Our results indicate that in order to design clathrates with low thermal conductivity, two physical quantities should be optimized: the charge transfer between the metal guest and the cages and the cage disorder induced by atomic substitution. In the absence of any atomic substitution, values of the lattice conductivity are twice as large and the system is metallic. We suggest that further reduction of the conductivity may be attained by forming clathrate superlattices where cages with different elements and rattlers are present in each portion. Work is in progress to realize various types of superlattices and to appropriately dope the clathrates so as to increase their electrical conductivity.

## AUTHOR INFORMATION


### Corresponding Author

*(G.G.) E-mail: gagalli@uchicago.edu.


### Notes

The authors declare no competing financial interest.

## ACKNOWLEDGMENTS

We thank Ding Pan, Éamonn Murray (E.M.), Fan Sui, and Susan Kauzlarich for useful discussions and E.M. for providing a code to calculate the partial phonon density of states. We gratefully acknowledge use of the computational facilities at NERSC at LBNL and funding from DOE/BES grant no. DE-FG02-06ER46262.

## REFERENCES


(1) Gaultois, M. W.; Sparks, T. D.; Borg, C. K. H.; Seshadri, R.; Bonificio, W. D.; Clarke, D. R. *Chem. Mater.* **2013**, *25*, 2911−2920.
(2) Tritt, T. M. *Annu. Rev. Mater. Res.* **2011**, *41*, 433−448.
(3) Snyder, G. J.; Toberer, E. S. *Nat. Mater.* **2008**, *7*, 105−114.
(4) Slack, G. A. *CRC Handbook of Thermoelectrics*; Rowe, D. M., Ed.; CRC Press: Boca Raton, FL, 1995; p 401.
(5) Nolas, G. S.; Cohn, J. L.; Slack, G. A.; Schujman, S. B. *Appl. Phys. Lett.* **1998**, *73*, 178−180.
(6) Cohn, J. L.; Nolas, G. S.; Fessatidis, V.; Metcalf, T. H.; Slack, G. A. *Phys. Rev. Lett.* **1999**, *82*, 779−782.
(7) Blake, N. P.; Møllnitz, L.; Kresse, G.; Metiu, H. *J. Chem. Phys.* **1999**, *111*, 3133−3144.
(8) Dong, J.; Sankey, O. F.; Ramachandran, G. K.; McMillan, P. F. *J. Appl. Phys.* **2000**, *87*, 7726−7734.
(9) Dong, J.; Sankey, O. F.; Myles, C. W. *Phys. Rev. Lett.* **2001**, *86*, 2361−2364.
(10) Tse, J. S.; Li, Z.; Uehara, K. *Europhys. Lett.* **2001**, *56*, 261−267.
(11) Okamoto, N. L.; Kim, J.-H.; Tanaka, K.; Inui, H. *Acta Mater.* **2006**, *54*, 5519−5528.
(12) Okamoto, N. L.; Tanaka, K.; Inui, H. *Mater. Res. Soc. Symp. Proc.* **2006**, *886*, 0886−F10−04.1.
(13) Christensen, M.; Abrahamsen, A. B.; Christensen, N. B.; Juranyi, F.; Andersen, N. H.; Lefmann, K.; Andreasson, J.; Bahl, C. R. H. *Nat. Mater.* **2008**, *7*, 811−815.
(14) Fujiwara, A.; Sugimoto, K.; Shih, C.-H.; Tanaka, H.; Tang, J.; Tanabe, Y.; Xu, J.; Heguri, S.; Tanigaki, K.; Takata, M. *Phys. Rev. B* **2012**, *85*, 144305.
(15) Christensen, S.; Bjerg, L.; Kaltzoglou, A.; Juranyi, F. *J. Appl. Phys.* **2013**, *113*, 084902.
(16) Bentien, A.; Christensen, M.; Bryan, J. D.; Sanchez, A.; Paschen, S.; Steglich, F.; Stucky, G. D.; Iversen, B. B. *Phys. Rev. B* **2004**, *69*, 045107.
(17) Christensen, M.; Iversen, B. B. *Chem. Mater.* **2007**, *19*, 4896−4905.
(18) Gatti, C.; Bertini, L.; Blake, N. P.; Iversen, B. B. *Chem.—Eur. J.* **2003**, *9*, 4556−4568.
(19) Nguyen, L. T. K.; Aydemir, U.; Baitinger, M.; Bauer, E.; Borrmann, H.; Burkhardt, U.; Custers, J.; Haghighirad, A.; Hofler, R.; Luther, K. D.; Ritter, F.; Assmus, W.; Grin, Y.; Paschen, S. *Dalton Trans.* **2010**, *39*, 1071−1077.
(20) Yan, X.; Grytsiv, A.; Giester, G.; Bauer, E.; Rogl, P.; Paschen, S. *J. Electron. Mater.* **2011**, *40*, 589−596.
(21) Bentien, A.; Palmqvist, A.; Bryan, J.; Latturner, S.; Stucky, G.; Furenlid, L.; Iversen, B. *Angew. Chem., Int. Ed.* **2000**, *39*, 3613−3616.
(22) He, Y.; Sui, F.; Kauzlarich, S. M.; Galli, G. *Energy Environ. Sci.* **2014**, DOI: 10.1039/C4EE00256C.
(23) Adams, G. B.; O'Keeffe, M.; Demkov, A. A.; Sankey, O. F.; Huang, Y.-M. *Phys. Rev. B* **1994**, *49*, 8048−8053.

(24) We optimized the structure of the $K_8Si_{46}$ clathrate and obtained site distances and an overall geometry in good agreement with experiments. Stefanoski, S.; Nolas, G. S. *Cryst. Growth Des.* **2011**, *11*, 4533. The lattice constant of the optimized model is 1.037 nm, 1% larger than the experimental value (1.026 nm).
(25) Giannozzi, P.; et al. http://www.quantum-espresso.org.
(26) Perdew, J. P.; Burke, K.; Ernzerhof, M. *Phys. Rev. Lett.* **1996**, *77*, 3865−3868.
(27) Perdew, J. P.; Burke, K.; Ernzerhof, M. *Phys. Rev. Lett.* **1997**, *78*, 1396−1396.
(28) Hamann, D. R.; Schlüter, M.; Chiang, C. *Phys. Rev. Lett.* **1979**, *43*, 1494−1497.
(29) Christensen, M.; Johnsen, S.; Iversen, B. B. *Dalton Trans.* **2010**, *39*, 978.
(30) Roudebush, J. H.; de la Cruz, C.; Chakoumakos, B. C.; Kauzlarich, S. M. *Inorg. Chem.* **2012**, *51*, 1805−1812.
(31) Giannozzi, P.; de Gironcoli, S. *Phys. Rev. B* **1991**, *43*, 7231−7242.
(32) Baroni, S.; de Gironcoli, S.; Corso, A. D. *Rev. Mod. Phys.* **2001**, *73*, 515−562.
(33) For all samples studied in this work, the DFPT calculations were carried out at the GGA level with the PBE functional. Perdew, J. P.; et al. *Phys. Rev. Lett.* **1997**, *78*, 1396. The Brillouin zone was sampled using a 4 × 4 × 4 *k*-point grid. The phonon dispersions were computed along the *x* direction using 20 points at the equilibrium geometry. The total and partial phonon density of states were computed with a 12 × 12 × 12 *q*-point grid.
(34) Ferry, D. K. *Semiconductors: Bonds and Bands*; IOP Publishing: Bristol, U.K>, 2013; pp 3−23.
(35) Mélinon, P.; Kéghélian, P.; Perez, A.; Champagnon, B.; Guyot, Y.; Saviot, L.; Reny, E.; Cros, C.; Pouchard, M.; Dianoux, A. J. *Phys. Rev. B* **1999**, *59*, 10099−10104.
(36) Euchner, H.; Pailhès, S.; Nguyen, L. T. K.; Assmus, W.; Ritter, F.; Haghighirad, A.; Grin, Y.; Paschen, S.; de Boissieu, M. *Phys. Rev. B* **2012**, *86*, 224303.
(37) He, Y.; Savic, I.; Donadio, D.; Galli, G. *Phys. Chem. Chem. Phys.* **2012**, *14*, 16209−16222.
(38) The thermal conductivity of the clathrates could in principle be obtained from approximate solutions of the Boltzmann transport equation in the single-mode relaxation time approximations: $\kappa_L = \Sigma_i c_i v_i^2 \tau_i$. While the group velocities ($v_i$) and single mode heat capacity ($c_i$) can be extracted from the phonon calculations, the evaluation of the mode lifetimes ($\tau_i$) from first principle is prohibitively expensive, from a computational standpoint, for a system with 54 atoms per unit cell. See, e.g., Savic, I.; et al. *Appl. Phys. Lett.* **2013**, *102*, 073113. Hence a kinetic model was used to estimate the conductivity.
(39) Sui, F.; Kauzlarich, S. Private communication.
(40) Hayashi, M.; Kishimoto, K.; Akai, K.; Asada, H.; Kishio, K.; Koyanagi, T. *J. Phys. D: Appl. Phys.* **2012**, *45*, 455308.